MOLECULAR IMAGING AND BIOLOGY

Mol Imaging Biol (2019) 21:973–983
DOI: 10.1007/s11307-018-1296-6

Published Online: 22 January 2019

RESEARCH ARTICLE

PET/CT Imaging of NSCLC with a $\alpha_v\beta_6$ Integrin-Targeting Peptide

Paul Flechsig,[1] Thomas Lindner,[1] Anastasia Loktev,[2] Saskia Roesch,[3] Walter Mier,[1] Max Sauter,[4] Michael Meister,[5] Christel Herold-Mende,[3] Uwe Haberkorn,[1,2] Annette Altmann[1,2]

[1]*Department of Nuclear Medicine, University Hospital Heidelberg, Heidelberg, Germany*
[2]*Clinical Cooperation Unit Nuclear Medicine, German Cancer Research Center (DKFZ), Heidelberg, Germany*
[3]*Division of Experimental Neurosurgery, Department of Neurosurgery, University Hospital Heidelberg, Heidelberg, Germany*
[4]*Department of Clinical Pharmacology and Pharmacoepidemiology, Heidelberg University Hospital, Heidelberg, Germany*
[5]*Department of Thoracic Oncology, University Hospital Heidelberg, Heidelberg, Germany*

Abstract

Purpose: Targeted therapies are regarded as promising approaches to increase 5-year survival rate of non-small cell lung cancer (NSCLC) patients. Here, we investigated the clinical value of the $\alpha_v\beta_6$ integrin-specific peptide SFITGv6 as a diagnostic reagent targeting NSCLC.

Methods: Affinity and binding properties of [^{125}I]SFITGv6 or [^{177}Lu]SFITGv6 for $\alpha_v\beta_6$ integrin-expressing NSCLC cell lines were evaluated in cell culture experiments including competition, kinetic, internalization, and efflux. To confirm $\alpha_v\beta_6$ integrin specificity *in vivo* small-animal positron emission tomography (PET) imaging using [^{68}Ga]SFITGv6 as radiotracer and biodistribution of [^{177}Lu]SFITGv6 in NCI-H2009 and NCI-H322 tumor-bearing mice was performed. Finally, to distinguish between benign and malignant lesions [^{68}Ga]SFITGv6 was applied as radiotracer for PET/x-ray computed tomography (CT) imaging of NSCLC patients with unclear diagnosis upon routinely performed 2-deoxy-2-[^{18}F]flouro-*D*-glucose ([^{18}F]FDG)-PET/CT. The biodistribution of the SFITGv6-ligand in different organs and tumor lesions of NSCLC patients was quantified 1 h and 3 h after injection measuring standard uptake values $(SUV)_{max}$.

Results: In vitro experiments revealed a significant time-dependent SFITGv6 binding of up to 33 % to $\alpha_v\beta_6$ integrin-expressing the cell lines NCI-H2009, NCI-H322, NCI-H292, NCI-H358, and high affinity ($IC_{50\text{-mean}}$ 3.1 nM) to NCI-H2009 and NCI-H322. Moreover, a fast internalization of approximately 66 % by NCI-H2009 and NCI-H322 cells was observed. Small-animal PET imaging and biodistribution experiments of NCI-H2009 and NCI-H322 xenografts demonstrated an increased tumor-specific accumulation of SFITGv6 40 to 60 min after injection. Finally, PET/CT scans of NSCLC patients after [^{18}F] FDG injection followed by [^{68}Ga]SFITGv6 application revealed correlating images. Comparing the uptake of [^{68}Ga]SFITGv6 and [^{18}F] FDG both PET/CT-examinations presented with significantly increased SUV_{max} values in histologically proven NSCLC lesions, but a generally higher accumulation of [^{18}F] FDG was noticed.

Electronic supplementary material The online version of this article (https://doi.org/10.1007/s11307-018-1296-6) contains supplementary material, which is available to authorized users.

Correspondence to: Paul Flechsig; *e-mail:* paul.flechsig@med.uni-heidelberg.de

Conclusions: Even if SFITGv6 demonstrates excellent affinity and specificity for $\alpha_v\beta_6$ integrin-expressing NSCLC cell lines and several NSCLC xenografts [^{18}F]FDG-PET/CT provides an advantage over [^{68}Ga]SFITGv6-PET/CT for the diagnosis of NSCLC patients.

Key words: $\alpha_v\beta_6$ integrin, PET/CT scan, [^{18}F] FDG, [^{68}Ga]SFITGv6, Non-small cell lung cancer, Peptide

Introduction

Carcinogenesis is often associated with genetic, epigenetic, and proteomic changes leading to an altered expression profile on the surface of cancer cells [1]. Based on the molecular difference between tumor cells and their non-malignant counterparts as well as on the identification of molecules with specificity for tumor cell-specific biomarkers, targeted therapies have successfully been developed [2]. In this regard, a special importance is attributed to phage display as a powerful tool to identify novel peptides with high specificity for a variety of molecules on tumor cells or on tumor neovasculature [3, 4]. Phage display on viable cells allows for the identification of tumor cell-specific peptides that have been successfully used as carriers for the delivery of therapeutic or imaging reagents even without knowing the exact target [5, 6]. Employing a sunflower trypsin inhibitor (SFTI)-1 based-phage display library for biopanning against head and neck (HNSCC)-derived tumor cells and corresponding PF2D membrane protein fractions, we previously identified the peptide SFITGv6 containing the $\alpha_v\beta_6$ integrin-specific binding motif arginine-glycine-aspartate (RGD) flanked by the LMQL sequence [7].

$\alpha_v\beta_6$ integrin is overexpressed in a variety of carcinomas associated with poor prognosis including pancreatic, ovarian, colorectal, and cervical cancer;, and in non-small cell lung cancer (NSCLC) [8–13], but only at low or undetectable levels in normal tissues. Therefore, $\alpha_v\beta_6$ integrin represents an important target for diagnostic imaging and anti-cancer therapies [14–20]. The peptide SFITGv6 provides excellent stability and high affinity for $\alpha_v\beta_6$ integrin (K_D 14.8 nM) but not for $\alpha_v\beta_3$ integin (K_D 185 nM). Correspondingly, SFITGv6 displayed specific binding to a variety of $\alpha_v\beta_6$ integrin-expressing epithelial tumor cells and accumulation in HNSCC tumors, but not to inflammatory lesions and healthy tissues of patients. Notably, excellent SFITGv6 uptake values were also noticed in tumor lesions of NSCLC patients. In addition, a strong tumor-specific histochemical peptide staining of brain metastasis derived from NSCLC (NCH2407) was observed [7] signifying the clinical value of SFITGv6 reagent targeting NSCLC.

Owing to the aggressive and highly metastatic potential and high recurrence rate lung cancer is a major cause of cancer-related death worldwide [21] and the 5-year survival rate of 15 % is still poor. NSCLC comprising adenocarcinoma (ADC), squamous cell carcinoma (SCC) and large cell carcinoma (LCLC) account for more than 80 % of all lung cancer cases a substantial proportion of which depends on oncogenic molecular aberrations [22]. Therefore, patients' outcome might be improved by better imaging tools for more precise tumor detection as well as by the help of targeted therapies allowing for a personalized approach according to the individual tumor genotype and phenotype.

Considering both, the requirement of improved imaging tools for lung cancer and the increased expression of $\alpha_v\beta_6$ integrin in NSCLC we investigated the clinical value of SFITGv6 as tracer for $\alpha_v\beta_6$ integrin-based positron emission tomography (PET) imaging in NSCLC patients.

Materials and Methods

Cell Lines and Culture Conditions

The human adenocarcinoma cell lines NCI-H2009, NCI-H358, and NCI-H322, the human mucoepidermoid pulmonary carcinoma cell line NCI-H292, the human large lung cell carcinoma cell lines NCI-H661, as well as the human squamous lung cell carcinoma cell line NCI-H1703 were obtained and authenticated by the American Type Culture Collection or by the German Collection of Microorganisms and Cell Cultures. All cell lines were negative for Mycoplasma and cultured in RPMI 1640 medium (Gibco) supplemented with 10 % fetal calf serum or in DMEM F12 medium (Gibco) supplemented with insulin (5 mg/μλ), transferrin (0.01 mg/ml), sodium selenite (30 nM), hydrocortisone (10 nM), β-estradiol (10 nM) and 5 % fetal calf serum (NCI-H2009) at 37 °C and 5 % CO_2.

Peptide Synthesis

For binding experiments and application in patients SFITGv6 was synthesized by Fmoc/tBU chemistry and labeled with Iodine-125 ([^{125}I]), Lutetium-177 ([^{177}Lu]), or Gallium-68 ([^{68}Ga]) (see electronic supplemental material: ESM).

In vitro Binding Experiments

NSCLC cells (2.5×10^5 to 4×10^5) were seeded in 6-well plates and cultivated for 48 h. For binding studies up to 60 min, the cells were incubated in 1 ml serum-free medium containing [^{125}I]SFITGv6. For competition

experiments the cells were simultaneously exposed to the I-125 labeled and the unlabeled peptide (10^{-5} M to 10^{-11} M). After washing 3 times with 1 ml phosphate-buffered saline (PBS; pH 7.4) the cells were lysed with 0.5 ml NaOH (0.3 M + 0.2 % SDS). Given that time-dependent deionization of [^{125}I]-labeled peptides might occur kinetic, internalization and efflux, respectively, were evaluated after exposure of the cells with [^{177}Lu]SFITGv6 for different time intervals (10 min to 240 min) and lysis with 0.5 ml NaOH (0.3 M). In particular, for the efflux experiment radioactive medium was replaced 60 min after exposure to [^{177}Lu]SFITGv6 by non-radioactive medium and cells were incubated again for 10 to 240 min before measuring radioactivity of the cell lysates and the medium. To evaluate peptide internalization, the cells were initially incubated with 1 ml of glycine-HCl (1 M) in PBS (pH 2.2) for 10 min to remove the surface bound activity, washed with 3 ml of ice-cold PBS and lysed with 0.5 ml NaOH (0.3 M). Radioactivity was determined in a gamma counter and calculated as percentage of the applied dose per 1×10^6 cells. Experiments were performed three times, and three repetitions per independent experiment were acquired.

Animals Studies

All experiments were conducted in compliance with the German animal protection laws. Eight-week-old Balb/c (nude/nude) mice obtained from Charles River Laboratories were inoculated subcutaneously at the right shoulder with 5 million tumor cells in MatriGel (BD Bioscience). For small-animal positron emission tomography (PET) imaging mice bearing NSCLC xenografts of 10–15 mm diameter were anesthetized using isoflurane inhalation and injected *via* tail-vein with 20 MBq [^{68}Ga]SFITGv6 (0.3–0.5 nmol) in 100 µl 0.9 % NaCl. For blocking experiments NSCLC xenografts were simultaneously injected with 50 µl aqueous solution (1 mM; 10 % DMSO; due to low solubility of the peptide) of unlabeled SFITGv6 (50 nmol) and 50 µl 20 MBq [^{68}Ga]SFITGv6 (0.3–0.5 nmol, approx. 50 MBq/nmol). DMSO is removed during the process of tracer preparation, so the clinical use is not limited. Images were recorded on an Inveon small-animal PET scanner (Siemens) using a 60 min emission scan in list mode and a 10 min transmission scan. Images were taken in 3-dimensional (3D) mode and reconstructed iteratively with a fully 3D algorithm from a 256×256 matrix for viewing transaxial, coronal, and sagittal slices of 0.9 mm thickness. Pixel size was $0.38 \times 0.38 \times 0.79$ mm^3 and transaxial resolution obtained was 0.9 mm. To assess the biodistribution, 100 µl of a 20 nM [^{177}Lu]SFITGv6 solution (1 MBq) was administered as an intravenous bolus injection into the tail vein. For each point of time (1, 2, 4, 24 h) we sacrificed three animals, collected peripheral blood and the respective organs, weighted the tissues, and measured the radioactivity using a γ-counter. Values were expressed as percentage of the injected dose radioactivity (MBq) per gram tissue (% ID/g).

PET/CT Imaging of Patients

This retrospective analysis of patient examinations was approved by the Institutional Review Board (IRB) and conducted according to the guidelines of the IRB and to good clinical practice according to the ethical principles that have their origin in the declaration of Helsinki. The requirement of informed consent was waived by the IRB. Patients with neoadjuvant radiation and/or chemotherapy were ruled out from the analysis. For reasons of therapy planning, 2-deoxy-2-[^{18}F]flouro-*D*-glucose ([^{18}F]FDG)-PET/x-ray computed tomography (CT) examinations were performed routinely according to the clinical schedule. Because of unclear imaging findings in [^{18}F]FDG-PET/CT, a total of nine lung cancer patients aged 50–76 years (8 male, median age 58 years) additionally underwent [^{68}Ga]SFITGv6-PET/CT-examinations within 2 weeks after [^{18}F]FDG-PET/CT for reasons of non-invasive differentiation between benign and malignant lesions according to clinical routine.

[^{18}F]FDG-PET/CT was performed after fasting for at least 8 h at a blood glucose level below 150 mg/dl, administering 4 MBq/kg body weight of [^{18}F] FDG intravenously 60 min in advance. Patients were examined with a Biograph mCT Flow PET/CT-Scanner (Siemens Medical Solution) using the following reconstruction parameters: slice thickness/reconstruction increment of 5.0/2.5 mm, standard soft-tissue reconstruction kernel B30, standard lung-tissue kernel k70. PET- and CT-data sets were reconstructed at a slice thickness/reconstruction increment of 5.0/2.5 mm.

[^{68}Ga]SFITGv6-PET/CT-examinations of the patients were performed 1 h and 3 h after intravenous injection of 4 MBq/kg body weight of [^{68}Ga]SFITGv6. Patients were examined with the same Biograph mCT Flow PET/CT-Scanner (Siemens Medical Solution) using the above-mentioned reconstruction parameters. Tracer uptake was quantified using standard uptake values $(SUV)_{max}$.

Statistical Analysis

Statistical analysis was performed using SigmaPlot (Systat Software GmbH) and R version (The R Foundation for Statistical Computing). Median and quantile values for SUV_{max} with 95 % confidence interval were calculated and illustrated in box-whisker plots. In order to account for possible correlations between lesions on the same patient, all statistical tests were performed by using likelihood-ratio tests in a linear mixed model, with "patient ID" as a random factor. All graphical displays refer to individual lesions. Differences were considered significant at $p < 0.05$ in a likelihood ratio test.

Results

High Affinity Binding of SFITGv6 to $\alpha_v\beta_6$ Integrin-Expressing NSCLC Cell Lines

First, we investigated the binding of the $\alpha_v\beta_6$ integrin-specific peptide SFITGv6 to different NSCLC cell lines *in vitro*. In accordance with the $\alpha_v\beta_6$ integrin expression profile (Suppl, Fig. 1, see ESM) [^{125}I]SFITGv6 demonstrated specific binding to the cell lines NCI-H2009 (up to 33 % ± 0.06), NCI-H358 (up to 18 % ± 0.27), NCI-H322 (up to 16 % ± 0.8), and to a lower extent to NCI-H292 (up to 13 % ± 0.7) within 60 min of exposure (Fig. 1a). In contrast, less than 1 % binding of the peptide was noticed to the cell lines NCI-H1703 characterized by low $\alpha v\beta_6$ integrin expression (Suppl. Fig. 1) and NCI-H661 (Fig. 1a). Based on this results, subsequent experiments concerning the detailed evaluation of binding properties and affinity of SFITGv6 to NSCLC cell lines *in vitro* including kinetics, internalization, efflux, and competition as well as the *in vivo* application was performed employing the NCI-H2009 and NCI-H322. To assess specificity and affinity of peptide binding a competition experiment was performed. Binding of [^{125}I]SFITGv6 to NCI-H2009 and NCI-H322 cells was almost completely competed by adding $10^{-}6$ M unlabeled counterparts demonstrating high affinity ($IC_{50\text{-mean}}$ 3.1 nM) of the peptide for these NSCLC cell lines (Fig. 1b).

Kinetic experiments revealed a continuously increasing binding of [^{177}Lu]SFITGv6 to NCI-H2009 (up to 12.4 % ± 0.097) and to NCI-H322 (up to 11.7 % ± 0.108) within 240 min (Fig. 1c). Approximately 66 % of the total bound peptide was internalized in the NSCLC cells. Concordantly, the efflux experiment demonstrated retention of more than 50 % of the originally accumulated SFITGv6 over 120 min after the termination of the uptake (Fig. 1d). Notably, a moderate renewed increase of SFITGv6 binding/internalization was

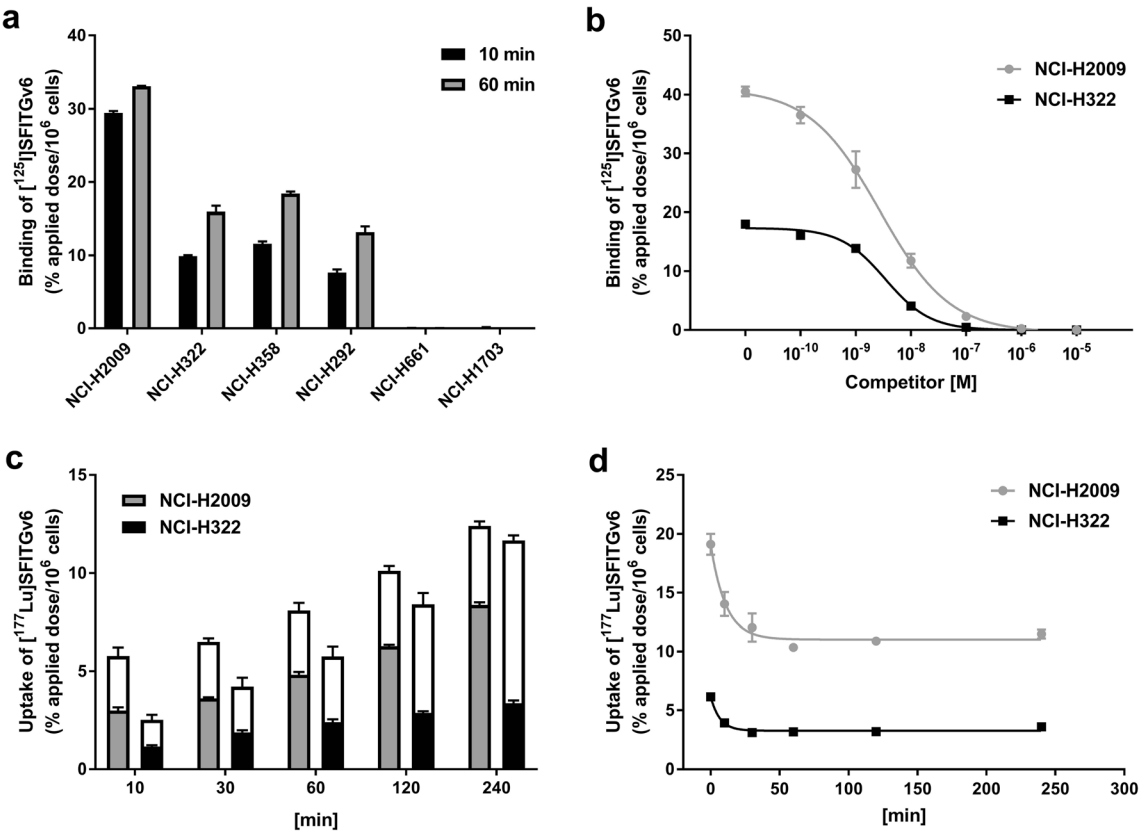

Fig. 1. *In vitro* characterization of SFITGv6 peptide: A binding of [^{125}I]SFITGv6 to different NSCLC cell lines (NCI-H2009, NCI-H322, NCI-H358, NCI-H292, NCI-H661, NCI-H1703), after exposure for 10 min (black bars) and for 60 min. B unlabeled SFITGv6 (10^{-10} M to 10^{-5} M) were used to compete for the binding of [^{125}I]SFITGv6 to NCI-H2009 and NCI-H292 cells within 60 min and the radioactivity was calculated as % applied dose/10^6 cells. C Total bound and internalized [^{177}Lu]SFITGv6 (black bars) in NCI-H2009 and NCI-H292 cells was determined after incubation for 10, 30, 60, 120, and 240 min, respectively. The internalized proportion is shown in black and gray, respectively; the extracellularly bound fraction is indicated by the white bar. D efflux of [^{177}Lu]SFITGv6 from NCI-H2009 and, NCI-H322 cells after incubation for 60 min. After replacement of the radioactive by non-radioactive medium the radioactivity in cell lysates was determined after 0, 1, 2, and 4 h. Generally, the radioactivity was calculated as percent applied dose/10^6 cells. Data represent mean values and standard derivation of triplicate measurements from representative experiment.

observed for both cell lines after 120 and 60 min, respectively, which might be explained by a peptide re-uptake from the culture medium (Fig. 1d).

Small-Animal PET/CT Imaging of NSCLC Xenografts

Small-animal PET imaging and biodistribution experiments of mice bearing NCI-H2009 (Fig. 2a, b, and c; Supplemental Fig. 2a–c) and NCI-H322 xenografts (Fig. 2d, e, and f; Suppl. Fig. 2d–f, see ESM) was performed to verify the $\alpha_v\beta_6$ integrin specificity and affinity of SFITGv6 *in vivo*. The images showed a fast and prominent accumulation of [^{68}Ga]SFITGv6 in the NCI-H2009 xenograft 20 to 40 min (Fig. 2a) after administration of the peptide (SUV_{mean} 0.45, Supplemental Fig. 2b) which was maintained for at least 140 min (Suppl. Fig. 2a). In contrast, small-animal PET imaging of the NCI-H322 xenograft bearing mouse revealed less, but also persisting peptide accumulation in the tumor (Fig. 2d, Suppl. Fig. 2d) correlating to a SUV_{mean} value of 0.32 (Suppl. Fig. 2e). In both NSCLC xenografts, specific accumulation of the radiolabeled peptide was inhibited if unlabeled SFITGv6 was simultaneously injected as competitor (Fig. 2b and e) correlating to SUV_{mean} values of 0.13 and 0.07, respectively, (Suppl. Fig. 2c, f). Generally, a rapid clearance of non-specific activity from the blood was noticed within 60 min after injection resulting in a low background and images with good tumor-to-background ratios. To expand on the biodistribution of [^{177}Lu]SFITGv6 radioactivity was measured in individual organs of NSCLC tumor-bearing mice after different time points following intravenous injection of [^{177}Lu]SFITGv6 and calculated as % ID/g (Fig. 2c and f). In accordance with the PET results, uptake of 1.5 % ID/g ± 0.36 and 1.7 % ID/g ± 0.13 in NCI-H2009 (Fig. 2c) and NCI-H322 xenografts (Fig. 2f), respectively, was measured 1 h after injection followed by a washout below 1 % ID/g after 24 h. However, a significantly higher uptake of 34.8 % ID/g ± 2.3 (NCI-H2009) and 42.6 % ID/g ± 2.6 (NCI-H322) with hardly any clearance was observed in the kidneys, whereas less than 1 % ID/g was

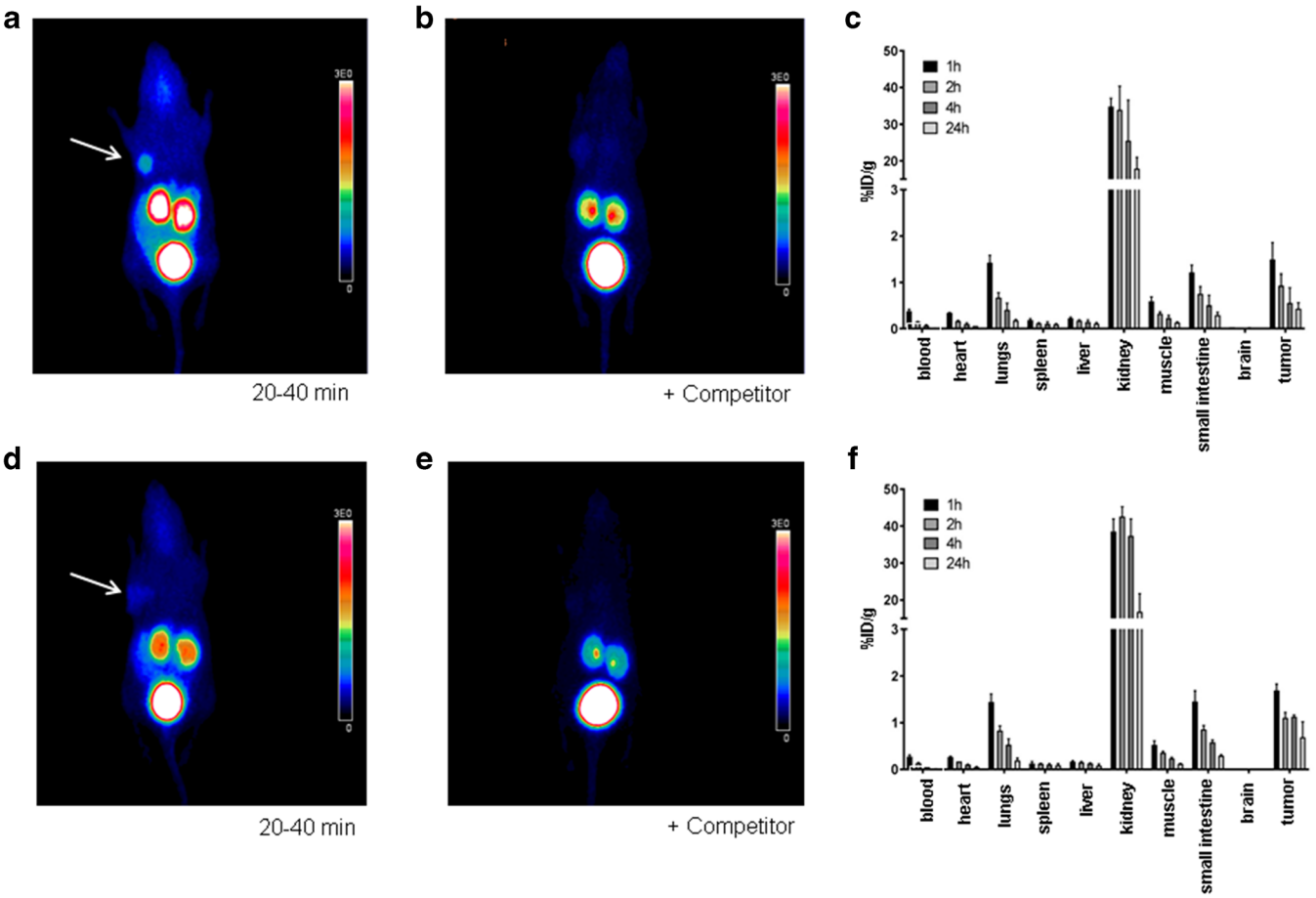

Fig. 2. Small-animal PET imaging of [^{68}Ga]SFITGv6 (20 MBq, 0.3–0.5 mM) localization in tumors of mice bearing A NCI-H2009 xenogafts and D NCI-H322 xenografts in the absence of blockade (100 µl 0.9 % NaCl). Localization was effectively blocked by co-injection of unlabeled SFITGv6 (1 mM, 50 µl aqueous solution/10 % DMSO) in B NCI-H2009 tumor and E NCI-H322 tumor. Biodistribution of [^{177}Lu]SFITGv6 in tumor and organs of C NCI-H2009, and F NCI-H322 tumor-bearing mice was measured 1, 2, 4, 24 h after injection and calculated as %ID/g. Data are mean of 3 mice per time point, error bars = standard derivation.

measured in the blood. Except for the kidneys, the tumor totissue ratios were above one (Supplemental Table 1).

Comparison of [^{18}F]FDG-PET/CT- and [^{68}Ga]SFITGv6-PET/CT-Scans in NSCLC Patients

Quantitative analyses of [^{68}Ga]SFITGv6-PET/CT were performed on the basis of histopathological gold standard, which was derived from tissue sampling along the clinical routine. Out of the 9 patients, a total of 19 histologically-assessed lesions could clearly be assigned to the respective [^{18}F]FDG-PET/CT- and [^{68}Ga]SFITGv6-PET/CT-scan. Among the 19 histologically proven lesions, histopathological findings were distributed as follows: 12 lesions were malignant (6 primary tumor, 5 lymph node metastasis (LN), and one distant metastasis). Out of them, six lesions were classified as squamous cell carcinoma (SQCC), three lesions as adenocarcinoma (ADC), and another three lesions as NOS (NSCLC not further classified due to sampling methodology *via* biopsy). Seven lesions were assessed as benign (six tumor-free and one hamartochondroma which is a benign mesenchymal cell-derived tumor of the lung).

In [^{68}Ga]SFITGv6-PET/CT, histologically proven malignant lesions presented with a mean SUV_{max} of 3.33 ± 1.7 1 h p.i., and a mean SUV_{max} of 2.9 ± 1.3 3 h p.i., which was significantly higher compared to tracer uptake of histologically proven benign lesions with a mean SUV_{max} of 1.24 ± 0.35 ($p < 0.05$) 1 h p.i., and a mean SUV_{max} of 1.0 ± 0.23 ($p < 0.05$) 3 h p.i. (Figs. 3, 4, and 5). Comparing tracer uptake in histologically proven malignant findings, both [^{68}Ga]SFITGv6 and [^{18}F]FDG-PET/CT examinations presented with significantly increased SUV_{max} values (Fig. 3), nevertheless the difference of SUV_{max} between malignant and benign lesions was bigger in [^{18}F]FDG-PET/CT compared to [^{68}Ga]SFITGv6-PET/CT ($p < 0.05$, Fig. 3). In the following, [^{68}Ga]SFITGv6 and [^{18}F]FDG-PET/CT examinations of two exemplarily chosen patients are demonstrated (Figs. 4 and 5). In order to simplify presentation of the findings, SUV_{max} values of both PET/CT scans are demonstrated for measurements at 1 h p.i.

Figure 4a shows [^{18}F]FDG-PET/CT and Fig. 4b shows [^{68}Ga]SFITGv6-PET/CT of a patient with ADC. Histopathology was derived from CT-guided core needle biopsy out of the primary tumor in the left lower lobe (lesion 3, blue circle) with high tracer accumulation in the primary tumor as revealed by [^{68}Ga]SFITGv6-(SUV_{max} 7.5) and [^{18}F]FDG-PET/CT (SUV_{max} 4.5). Besides the histopathologically proven primary tumor, [^{18}F]FDG-PET/CT revealed findings suspicious for tumor spread in the following localizations: mediastinal LNs (lesion 2, green circle, [^{18}F]FDG-PET/CT:

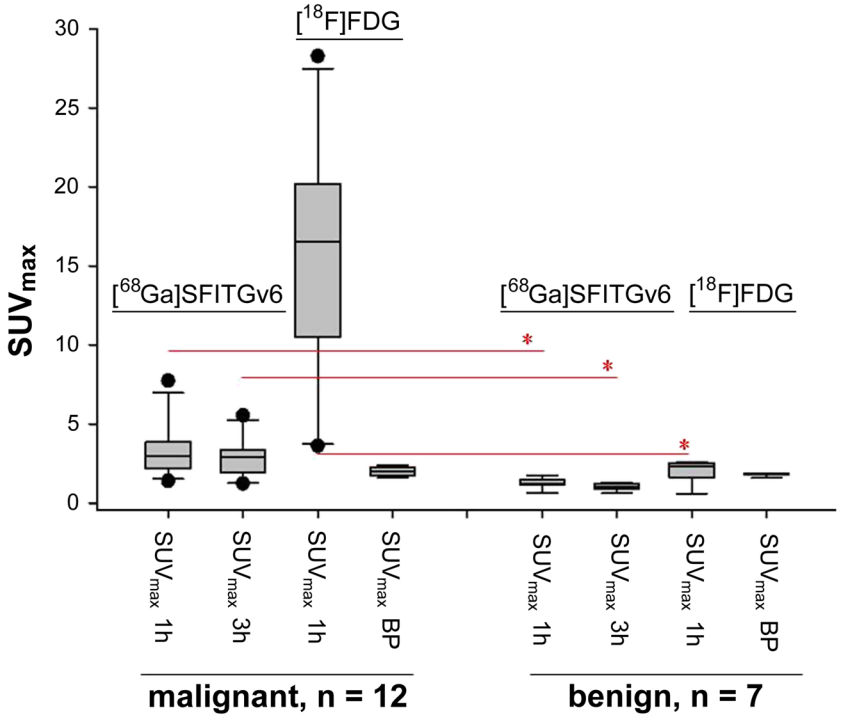

Fig. 3. Uptake of [^{18}F] FDG and [^{68}Ga]SFITGv6 in the PET/CT malignant (left columns) and benign (right columns) lesions (boxplots with median, 25 % and 75 %-quartiles, and 95 % confidence interval). Left columns: SUV_{max} in histologically proven malignant lesions for [^{68}Ga]SFITGv6-PET/CT 1 h and 3 h p.i., and for [^{18}F]FDG-PET/CT 1 h p.i. with additional measurement of mediastinal blood pool (BP) 1 h p.i. Right columns: SUV_{max} in benign lesions for [^{68}Ga]SFITGv6-PET/CT 1 h and 3 h p.i., and for [^{18}F]FDG-PET/CT 1 h p.i. with additional measurement of mediastinal blood pool (BP) 1 h p.i. Red stars indicate statistically significant differences of tracer uptake between malignant and benign lesions ($p < 0.05$).

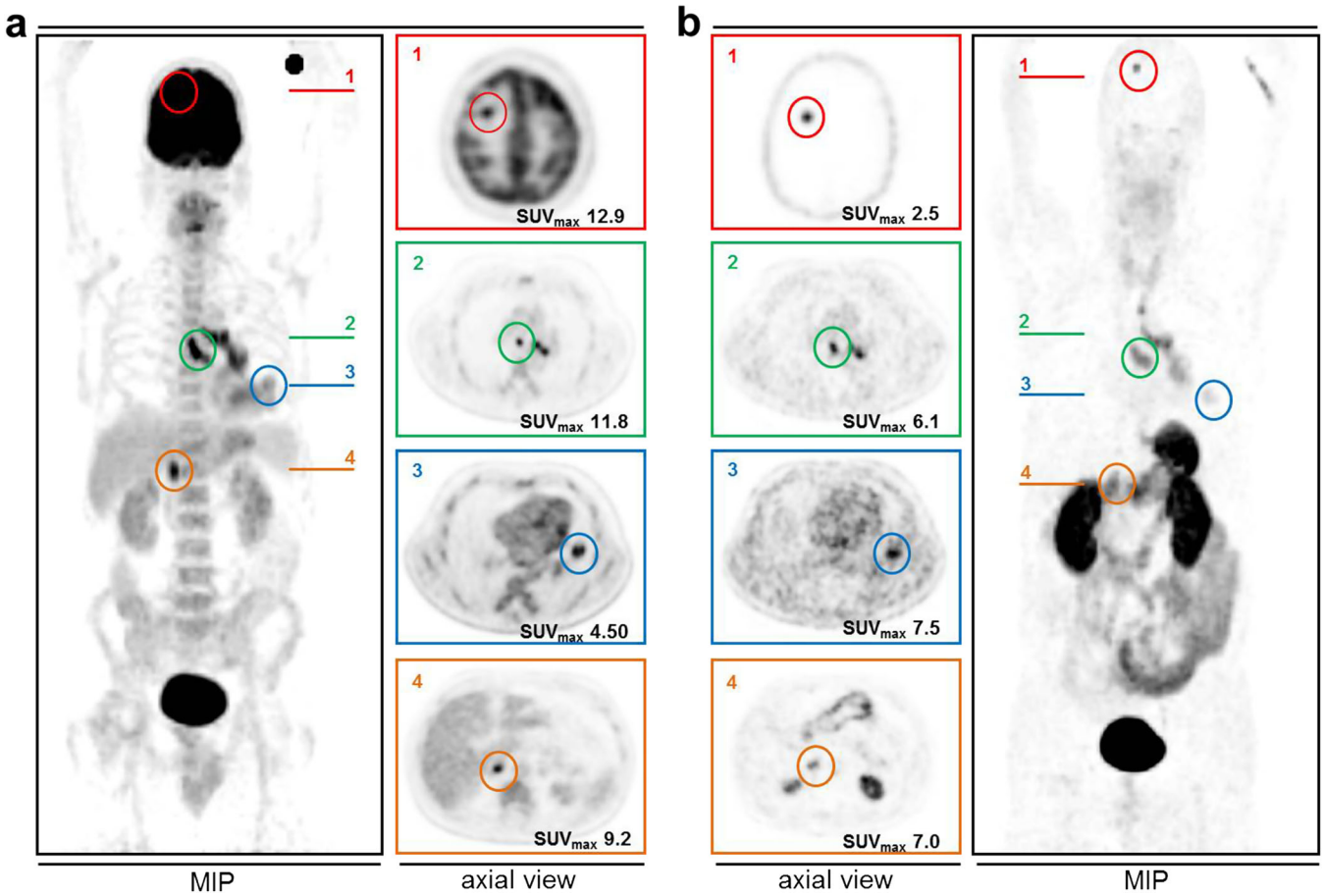

Fig. 4. PET/CT scan of the 1. NLCLC patient 1 h after application of A [^{18}F] FDG and B [^{68}Ga]SFITGv6. Respective SUV_{max} is stated on the right lower bottom of colored frames (lesion 1: brain metastasis, lesion 2: loco-regional LN-metastases, lesion 3: histologically proven primary tumor in the left lower lobe, lesion 4: distant metastasis in the right adrenal gland).

SUV_{max} 11.8, [^{68}Ga]SFITGv6-PET/CT: SUV_{max} 6.1), brain (lesion 1, red circle, [^{18}F]FDG-PET/CT: SUV_{max} 12.9, [^{68}Ga]SFITGv6-PET/CT: SUV_{max} 2.5), and right adrenal gland (lesion 4, orange circle, [^{18}F]FDG-PET/CT: SUV_{max} 9.2, [^{68}Ga]SFITGv6-PET/CT: SUV_{max} 7.0). Notably, we observed low physiological uptake of [^{68}Ga]SFITGv6 in the brain as compared to [^{18}F] FDG improving visibility of intracerebral metastases.

In Fig. 5, [^{18}F]FDG-PET/CT (left) and [^{68}Ga]SFITGv6-PET/CT (right) are shown in a patient with histologically proven ADC out of a bone metastasis in the right femur (lesion 4, orange circle, [^{18}F]FDG-PET/CT: SUV_{max} 20.6, [^{68}Ga]SFITGv6-PET/CT: SUV_{max} 7.9). According to the [^{18}F]FDG-PET/CT, the primary tumor is located in the right lower lobe (lesion 3, blue circle, [^{18}F]FDG-PET/CT: SUV_{max} 12.6, [^{68}Ga]SFITGv6-PET/CT: SUV_{max} 2.4, note poor visibility in MIP of [^{68}Ga]SFITGv6-PET due to high physiological kidney uptake, improved visibility in axial slices (green frame)). Moreover, suspicious findings for LN metastases were found in the right hilum (lesion 2 in position 10R, green circle, [^{18}F]FDG-PET/CT: SUV_{max} 5.8, [^{68}Ga]SFITGv6-PET/CT: SUV_{max} 1.8; again poor visibility in MIP due to high kidney uptake, visible in axial slices). Multifocal intensive tracer accumulations in the thyroid gland (lesion 1a and 1b, red circes [^{18}F]FDG-PET/CT: SUV_{max} 13.8 (lesion 1a), [^{68}Ga]SFITGv6-PET/CT: SUV_{max} 10.6 (lesion 1a) turned out to be autonomous adenomas of the thyroid gland during ultrasound and external scintigraphy.

Biodistribution and Tracer-Uptake in the [^{68}Ga]SFITGv6-PET/CT-Examination

Biodistribution of the SFITGv6-ligand was measured 60 min and 3 h p.i., and quantified by measuring the SUV_{max}. An intense accumulation in the kidneys, gut and intestine was measured 60 min and 3 h p.i., only low uptake was found in parenchymal organ tissues, *e.g.* in the liver, as well as the brain (Fig. 6a and b), which might potentially be beneficial for the detection of liver- and brain metastases due to low physiological background in above mentioned organs (also see brain metastasis of patient with ADC in Fig. 3).

Discussion

Radiolabeled peptides for diagnosis and targeted therapy of tumors are characterized by efficient transport to the tumor

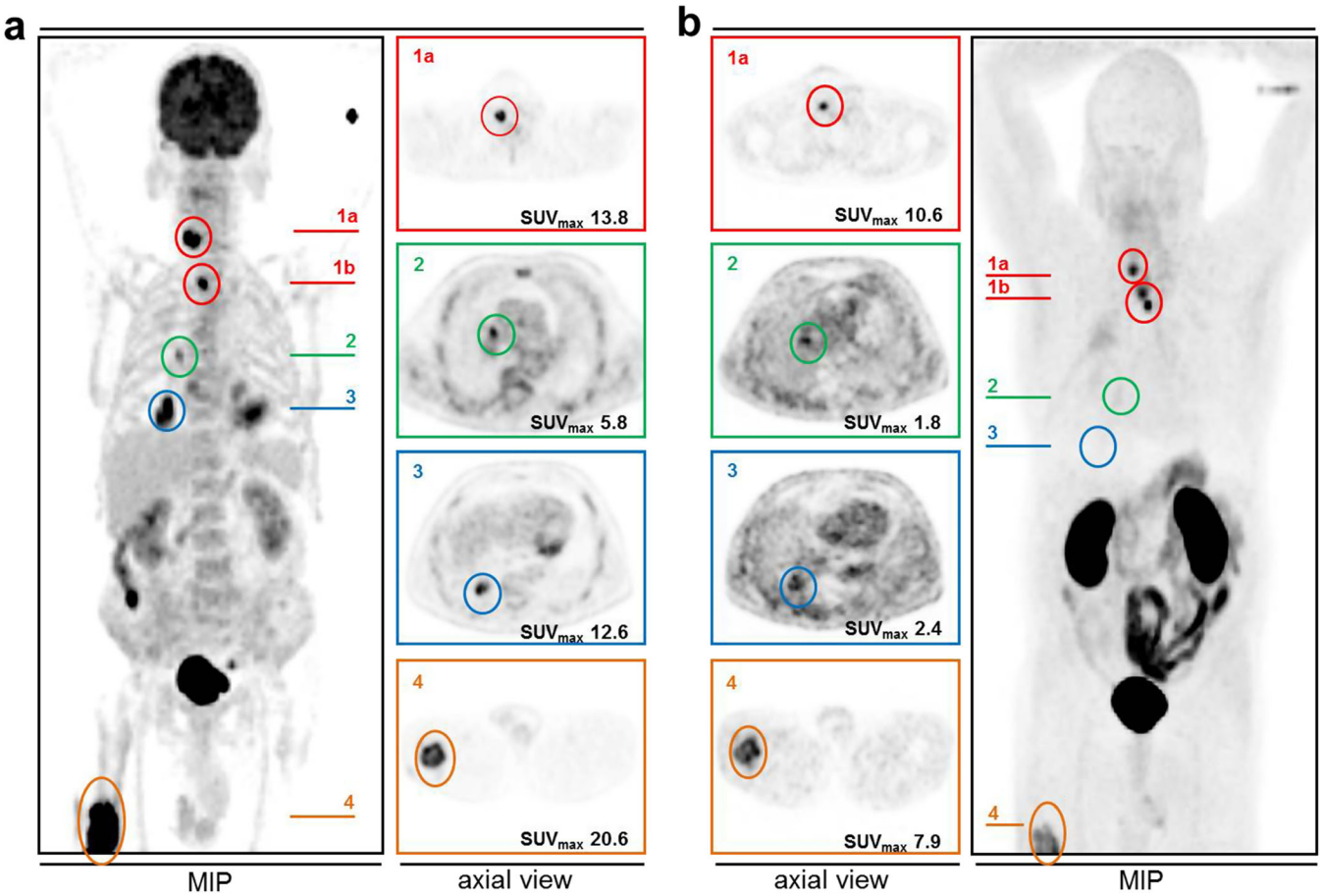

Fig. 5. PET/CT scan of 2. NLCLC patient 1 h after the application of A [^{18}F] FDG and B [^{68}Ga]SFITGv6. Respective SUV_{max} is stated on the right lower bottom of colored frames (lesion 1a and 1b: autonomous adenomas of thyroid gland, lesion 2: loco-regional LN-metastasis, lesion 3: primary tumor in the right lower lobe, lesion 4: histologically proven distant metastasis in the right femur).

cells and a fast clearance from the organism. Recently, target-specific peptides embedded in disulfide-stabilized scaffolds have been identified by phage display technologies or engineering that specifically target the angiogenesis marker delta-like ligand 4 [4] or $\alpha_v\beta_6$ integrin expressed on pancreatic tumor cells and HNSCC [7, 16, 23]. Given that $\alpha_v\beta_6$ integrin is overexpressed in a variety of epithelial tumors including lung carcinoma associated with poor prognosis, we investigated the potential of the previously $\alpha_v\beta_6$ integrin-specific peptide SFITGv6 as diagnostic tool for the detection of primary as well as NSCLC-derived metastasis *in vitro* and *in vivo*.

As expected from the binding properties of SFITGv6 for a variety of $\alpha_v\beta_6$ integrin-expressing tumor cell lines including lung carcinoma cells and for NSCLC-derived brain metastasis [7] we demonstrated significant peptide binding of the up to 33 % to NSCLC cell lines. Peptide binding correlated well to the $\alpha_v\beta_6$ integrin expression profile of individual cell lines. Subsequent competition experiments on NCI-H2009 and NCI-H322 cells confirmed specificity and demonstrated high affinity ($IC_{50\text{-mean}}$ 3.1 nM) of SFITGv6 for $\alpha_v\beta_6$ integrin. Notably, these cells also revealed significant internalization of almost 66 % of total bound [^{177}Lu]SFITGv6 and less than 50 % efflux of the originally accumulated peptide over the time period of 240 min, signifying a long-lasting peptide accumulation in NSCLC cells which justifies further *in vivo* evaluation.

In fact, based on an excellent tumor to background ratio, we successfully and selectively imaged NCI-H2009 xenograft in small animal PET scans for at least 140 min using [^{68}Ga]SFITGv6 as radiotracer. As expected from the *in vitro* binding properties of SFITGv6 for NCI-H322 cells and the $\alpha_v\beta_6$ integrin expression profile less, but also persisting accumulation of the [^{68}Ga]-labeled peptide was noticed in the small-animal PET imaging of NCI-H322 xenografts. Recently, significant differences in [^{68}Ga]SFITGv6 accumulation in $\alpha_v\beta_6$ integrin-expressing HNSCC xenografts were observed [7, 24] emphasizing the importance of pronounced target expression for the selective tumor imaging/targeting. However, binding of

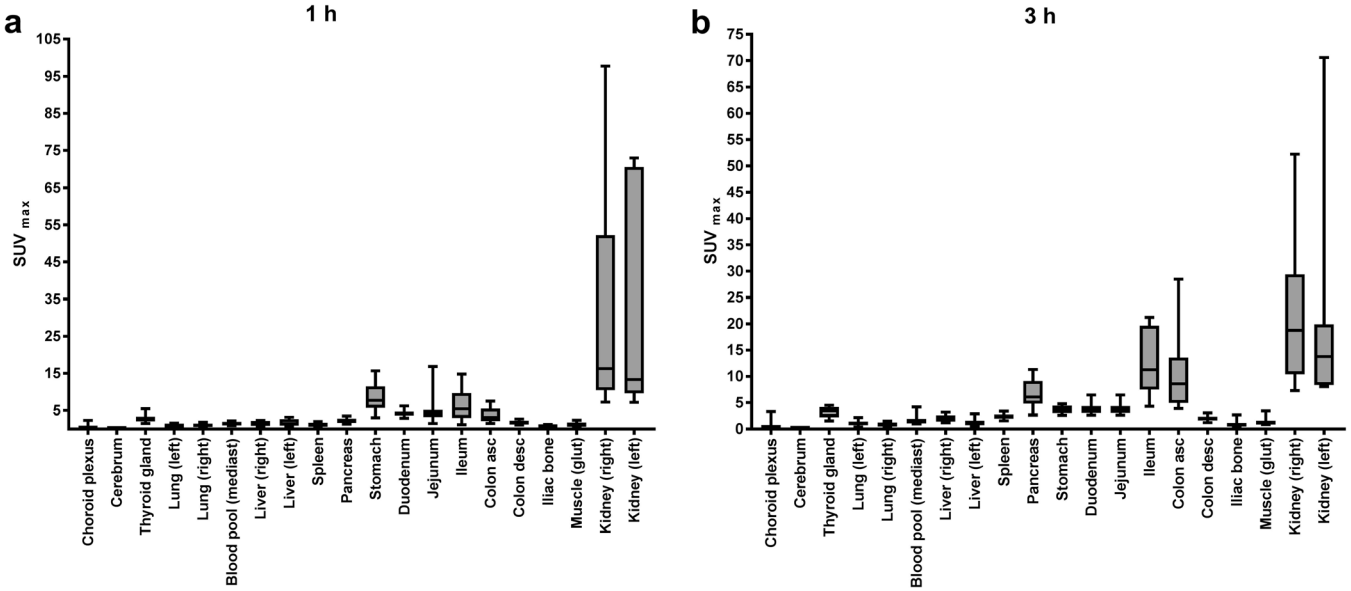

Fig. 6. Biodistribution of SFITGv6-PET/CT (box-plots with median, 25 % and 75 %-quartiles and 95 % confidence interval) A 1 h p.i. with highest tracer accumulation in the excretory organs (kidneys, in the gut, as well as the intestine, especially ileum and ascending colon). Low-tracer accumulation in the brain, as well as the abdominal parenchymal organs including liver, pancreas, and spleen and B 3 h p.i. with lower tracer accumulation in the kidneys compared to the measurement 1 h p.i., but now increased tracer uptake in ileum and ascending colon. Comparable to the measurement 1 h p.i. low tracer accumulation in the brain, as well as the abdominal parenchymal organs including liver, pancreas, and spleen.

[^{68}Ga]SFITGv6 to both NSCLC xenografts was almost completely prevented by simultaneous injection of the non-radioactive analog confirming $\alpha_v\beta_6$ integrin specificity of SFITGv6 *in vivo*. In accordance with the PET results, significant accumulation of [^{177}Lu]SFITGv6 in NCI-H2009 (1.5 % ID/g) and NCI-H322 xenografts (1.7 % ID/g) was noticed 1 h after injection followed by a rapid washout of the radioactivity within 4 h. For comparison, SFITGv6 displayed a significantly higher accumulation in NCI-H2009 tumors but also in the kidneys, muscle and intestine of NCI-H2009 tumor-bearing mice than the $\alpha_v\beta_6$ integrin-selective peptide cyclo (FRGDLAFp (*N*Me) K [25]. Using [^{99}Tc]-labeled H2009.1 conjugate [26] and the PEGylated A20FMDV2 variant [^{18}F]FBA-PEG28-A20FMDV2 [27] as $\alpha_v\beta_6$ integrin-specific radiotracer less or comparable tumor uptake of 0.88 % ID/g and 1.88 % ID/g, respectively, was measured in the pancreatic tumor model BcPC3.

Of particular interest is the high and persisting level of radioactivity of 35 % to 43 % ID/g in the kidneys of NSCLC xenografts. Kidney retention of radiolabeled peptidic probes is an often observed and complicated multifactorial issue depending on stability, charge, hydrophobicity and chemical modifications of the peptide [2, 14, 27]; for therapeutic application of radiolabeled peptides reduction of kidney retention is required.

Nevertheless, the high affinity and binding of SFITGv6 to $\alpha_v\beta_6$ integrin-expressing NSCLC cell lines *in vitro* and NSCLC xenografts *in vivo* and the excellent proteolytic stability of SFITGv6 [7] compared to cyclo (FRGDLAFp (*N*Me) K [25] and linear peptides encouraged us to evaluate the potential of the peptide as additional diagnostic tracer for NSCLC patients with unclear imaging findings based on [^{18}F]FDG-PET/CT. With regard to the detection of tumor lesions in NSCLC patients, [^{68}Ga]SFITGv6-PET/CT examinations demonstrated an increased SUV_{max} in histologically proven malignant lesions compared to the benign ones. However, [^{18}F]FDG-PET/CT revealed an advantage over [^{68}Ga]SFITGv6-PET/CT. As stated in several recently published data, [^{18}F]FDG-PET/CT is one of the most widespread and reliable imaging methodologies in non-invasive lung cancer staging, especially for reasons of pre-therapeutic TNM-staging [28]. Nevertheless, false positive findings can occur, since the scan can record inflammation due to infectious lung diseases, which is a clinically important draw back especially for mediastinal N-staging [29]. In these cases, [^{68}Ga]SFITGv6-PET/CT might serve as an additional tool to distinguish between malignant lesions and inflammatory lesions, thus helping to close the diagnostic gap in [^{18}F]-FDG-PET/CT-based lung cancer staging. In addition, a diagnostic gap in slow-growing lepidic adenocarcinomas with missing increase of [^{18}F]FDG uptake can result in false negative PET findings [28]. Also in neuroendocrine tumors of high differentiation with increased somatostatin receptors, an additional somatostatin receptor scintigraphy, or DOTATOC-PET/CT can be necessary to complete TNM-staging [30], which

encourages for the complemented use of somatostatin receptor imaging and [^{18}F]FDG-PET/CT in order to display the true differentiation of unclear lung lesions [31–33]. In the above-mentioned cases of false positive and false negative findings in [^{18}F]FDG-PET/CT, [^{68}Ga]SFITGv6-PET/CT might potentially help to further distinguish between a malignant and benign histopathology. Yet, this hypothesis could not be proven in this present analysis, and should be further evaluated in a prospective trial.

Conclusion

Investigating the potential of SFITGv6 as a tracer for NSCLC, we present a peptide providing high binding for $\alpha_v\beta_6$ integrin-expressing NSCLC cell lines *in vitro* and NSCLC xenografts *in vivo*. Given that the clinical value of peptide-based tracers as diagnostic tracer strongly depends on the target expression profile on tumor lesions, [^{68}Ga]SFITGv6-PET/CT-scan could be used to clearly distinguish between malignant and inflammatory lesions but not substitute for the [^{18}F]FDG-PET/CT-based diagnosis of NSCLC tumor lesions.

Acknowledgements. We thank Vanessa Kohl and Marlene Tesch for technical assistance as well as Irina Kupin and Karin Leotta for performing the animal experiments.

FundingThis project was supported by the Deutsche Forschungsgemeinschaft (DFG) [HA 2901/12-1].

Compliance with Ethical Standards

Conflict of Interest

The authors declare no conflict of interest.

References

1. Sekido Y, Fong KM, Minna JD (2003) Molecular genetics of lung cancer. Annu Rev Med 54:73–87
2. Weiner RE, Thakur ML (2005) Radiolabeled peptides in oncology: role in diagnosis and treatment. BioDrugs 19:145–163
3. Man YKS, DiCara D, Chan N, Vessillier S, Mather SJ, Rowe ML, Howard MJ, Marshall JF, Nissim A (2013) Structural guided scaffold phage display libraries as a source of bio-therapeutics. PLoS One 8:e70452
4. Zoller F, Markert A, Barthe P, Zhao W, Weichert W, Askoxylakis V, Altmann A, Mier W, Haberkorn U (2012) Combination of phage display and molecular grafting generates highly specific tumor-targeting miniproteins. Angew Chem Int Ed 51:13136–13139
5. Koivunen E, Arap W, Rajotte D, Lahdenranta J, Pasqualini R (1999) Identification of receptor ligands with phage display peptide libraries. J Nucl Med 40:883–888
6. Nothelfer EM, Zitzmann-Kolbe S, Garcia-Boy R, Kramer S, Herold-Mende C, Altmann A, Eisenhut M, Mier W, Haberkorn U (2009) Identification and characterization of a peptide with affinity to head and neck cancer. J Nucl Med 50:426–434
7. Altmann A, Sauter M, Roesch S, Mier W, Warta R, Debus J, Dyckhoff G, Herold-Mende C, Haberkorn U (2017) Identification of a novel the ITGαvβ6-binding peptide using protein separation and phage display. Clin Cancer Res 23:4170–4180
8. Sipos B, Hahn D, Carceller A, Piulats J, Hedderich J, Kalthoff H, Goodman SL, Kosmahl M, Kloppel G (2004) Immunohistochemical screening for β6-integrin subunit expression in adenocarcinomas using a novel monoclonal antibody reveals strong up-regulation in pancreatic ductal adenocarcinomas in vivo and in vitro. Histopathology 45:226–236
9. Ahmed N, Riley C, Rice GE, Quinn MA, Baker MS (2002) αvβ6 integrin-a marker for the malignant potential of epithelial ovarian cancer. J Histochem Cytochem 50:1371–1379
10. Bates RC, Bellovin DI, Brown C, Maynard E, Wu B, Kawakatsu H, Sheppard D, Oettgen P, Mercurio AM (2005) Transcriptional activation of integrin β6 during the epithelial-mesenchymal transition defines a novel prognostic indicator of aggressive colon carcinoma. J Clin Invest 115:339–347
11. Hazelbag S, Kenter GG, Gorter A, Dreef EJ, Koopman LA, Violette SM, Weinreb PH, Fleuren GJ (2007) Overexpression of the alpha v beta 6 integrin in cervical squamous cell carcinoma is a prognostic factor for decreased survival. J Pathol 212:316–324
12. Elayadi AN, Samli KN, Prudkin L, Liu YH, Bian A, Xie XJ, Wistuba II, Roth JA, McGuire MJ, Brown KC (2007) A peptide selected by biopanning identifies the integrin αvβ6 as a prognostic biomarker for nonsmall cell lung cancer. Cancer Res 67:5889–5895
13. Berghoff AS, Kovande AK, Melchardt T et al (2014) αvβ3, αvβ5 and αvβ6 integrins in brain metastases of lung cancer. Clin Exp Metastasis 31:841–851
14. Singh AN, McGuire MJ, Li S et al (2014) Dimerization of a phage-display selected peptide for imaging of αvβ6-integrin: two approaches to the multivalent effect. Theranostics 4:745–760
15. Hu LY, Bauer N, Knight LM, Li Z, Liu S, Anderson CJ, Conti PS, Sutcliffe JL (2014) Characterization and evaluation of ^{64}Cu-labeled A20FMDV2 conjugates for imaging the integrin αvβ6. Mol Imaging Biol 16:567–577
16. Hackel BJ, Kimura RH, Miao Z, Liu H, Sathirachinda A, Cheng Z, Chin FT, Gambhir SS (2013) ^{18}F-fluorobenzoate–labeled cystine knot peptides for PET imaging of integrin αvβ6. J Nucl Med 54:1101–1105
17. Zhu X, Li J, Hong Y, Kimura RH, Ma X, Liu H, Qin C, Hu X, Hayes TR, Benny P, Gambhir SS, Cheng Z (2014) ^{99m}Tc-labeled cystine knot peptide targeting integrin αvβ6 for tumor SPECT imaging. Mol Pharm 11:1208–1217
18. John AE, Luckett JC, Tatler AL, Awais RO, Desai A, Habgood A, Ludbrook S, Blanchard AD, Perkins AC, Jenkins RG, Marshall JF (2013) Preclinical SPECT/CT imaging of αvβ6 integrins for molecular stratification of idiopathic pulmonary fibrosis. J Nucl Med 54:2146–2152
19. White JB, Boucher DL, Zettlitz KA, Wu AM, Sutcliffe JL (2015) Development and characterization of an αvβ6-specific diabody and a disulfide-stabilized αvβ6-specific cys-diabody. Nucl Med Biol 42:945–957
20. Hausner SH, Bauer N, Hu LY, Knight LM, Sutcliffe JL (2015) The effect of bi-terminal PEGylation of an integrin $\alpha v\beta_6$-targeted ^{18}F peptide on pharmacokinetics and tumor uptake. J Nucl Med 56:784–790
21. Siegel RL, Miller KD, Jemal A et al (2015) Cancer statistics, 2015. CA Cancer J Clin 58:71–96
22. Rothschid SI (2015) Targeted therapies in non-small cell lung cancer-beyond EGFR andALK. Cancer 7:930–949
23. Kimura RH, Teed R Hackel BJ et al (2012) Pharmacokinetically stabilized cysteine knot peptides that bind alpha-vbeta-6 integrin with single-digit nanomolar affinities for detection of pancreatic cancer. Clin Cancer Res 18:839–840
24. Roesch S, Lindner T, Sauter M (2018) Comparative study of the novel RGD motif-containing αvβ6 integrin binding peptides SFLAP3 and SFITGv6 for diagnostic application in HNSCC. J Nucl Med in press
25. Notni J, Reich D, Maltsev OV, Kapp TG, Steiger K, Hoffmann F, Esposito I, Weichert W, Kessler H, Wester HJ (2017) In vivo PET imaging of the cancer integrin αvβ6 using ^{68}Ga-labeled cyclic RGD nonapeptides. JNM 58:671–677

26. Liu Z, Liu H, Ma T, Sun X, Shi J, Jia B, Sun Y, Zhan J, Zhang H, Zhu Z, Wang F (2014) Integrin $\alpha_v\beta_6$-targeted SPECT imaging for pancreatic cancer detection. JNM 55:989–994
27. Hausner SH, Abbey CK, Bold RJ, Gagnon MK, Marik J, Marshall JF, Stanecki CE, Sutcliffe JL (2009) Targeted in vivo imaging of integrin alphavbeta6 with an improved radiotracer and its relevance in a pancreatic tumor model. Cancer Res 69:5843–5850
28. Flechsig P, Mehndiratta A, Haberkorn U, Kratochwil C, Giesel FL (2015) PET/MRI and PET/CT in lung lesions and thoracic malignancies. Semin Nucl Med 45:268–281
29. Flechsig P, Kratochwil C, Schwartz LH, Rath D, Moltz J, Antoch G, Heussel CP, Rieser M, Warth A, Zabeck H, Kauczor HU, Haberkorn U, Giesel FL (2014) Quantitative volumetric CT-histogram analysis in N-staging of 18F-FDG-equivocal patients with lung cancer. J Nucl Med 55:559–564
30. Dimitrakopoulou-Strauss A, Georgoulias V, Eisenhut M, Herth F, Koukouraki S, Mäcke HR, Haberkorn U, Strauss LG (2006) Quantitative assessment of SSTR2 expression in patients with non-small cell lung cancer using ^{68}Ga-TOC PET and comparison with ^{18}F-FDG PET. Eur J Nucl Med Mol Imaging 33:823–830
31. Naalsund A, Maublant J (2006) The solitary pulmonary nodule–is it malignant or benign? Diagnostic performance of Tc-depreotide SPECT. J Respiration 73:634–641
32. Halley A, Hugentobler A, Icard P, Porret E, Sobrio F, Lerochais JP, Bouvard G, Zalcman G, Agostini D (2005) Efficiency of ^{18}F-FDG and ^{99m}Tc-depreotide SPECT in the diagnosis of malignancy of solitary pulmonary nodules. Eur J Nucl Med Mol Imaging 32:1026–1032
33. Menda Y, Kahn D (2002) Somatostatin receptor imaging of non-small cell lung cancer with ^{99m} Tc depreotide. Semin Nucl Med 32:92–96